Dynamics of plumes driven by localized heating in a stably stratified ambient

Juan M. Lopez[1] and Francisco Marques[2]

[1]School of Mathematical and Statistical Sciences,
Arizona State University, Tempe, Arizona
jmlopez@asu.edu
[2]Departament de Física Aplicada,
Universitat Politècnica de Catalunya, Barcelona
francisco.marques@upc.es

Abstract

The transition from laminar to complex spatio-temporal dynamics of a plume driven by a localized heat source at the bottom of an enclosed cylinder whose sidewall is maintained at a fixed temperature which varies linearly up the wall is studied. Restricting the dynamics to the axisymmetric subspace, the first instability is to a puffing state. However, for smaller Grashof numbers, the plume becomes unstable to three-dimensional perturbations and a swirling plume spontaneously appears. The next bifurcation also exhibits puffing and suggests a connection between the unstable axisymmetric puffing solution and the swirling plume. Further bifurcations result in quasi-periodic states with a very low-frequency modulation, and these eventually become spatio-temporally complex.

1 Introduction

Plumes due to localized buoyancy sources are of wide interest due to their prevalence in many geophysical situations. Several experiments have reported that this transition is sensitive to external perturbations. The present study was motivated by the long-standing puzzle that for many plumes, including some geophysical plumes, swirl is sometimes observed, and yet there is not a generally accepted explanation of where it comes from, particularly for plumes whose scales are such that the Coriolis force is not expected to be a primary factor. For the most part, explanations rely on the focusing and amplification of background rotation or shear near the ground by the updraft from the plume. The important issue is to determine if the swirl arises due to extraneous effects (ambient rotation or ambient shear) or due to intrinsic effects. One way to determine this is to eliminate external disturbances, and this is done by employing an enclosed geometry. The laboratory experiments of Torrance (1979) considered a plume in a completely enclosed cylinder driven by a localized hot spot on the bottom boundary. In a parameter regime where the ambient stratification is not too weak or too strong, the onset of swirl in the plume was observed, but no details of the flow nor any explanation of what the swirl was due to were offered. Nevertheless, the completely enclosed experiments suggest that the onset of swirl could be intrinsic to the plume dynamics.

2 Governing equations and numerical technique

Consider a cylinder of radius R and length L, with an imposed temperature profile at the cylinder wall. The bottom endwall has a fixed temperature T_0^* except for a disk of diameter D at the bottom center with a hotter temperature T_h^*. The top endwall is kept at a temperature T_t^*, and the temperature varies linearly along the sidewall between T_0^*

at the bottom and T_t^* at the top, resulting in a stable stratification, except for the hot spot at the bottom. The Brunt-Väisälä frequency $N_{\rm BV}$ is

$$N_{\rm BV}^2 = -(g/\rho_0)d\rho(z^*)/dz^* = \rho_0\alpha(T_t^* - T_0^*)/L, \tag{1}$$

where α is the coefficient of thermal expansion and ρ_0 is the density at temperature T_0^*.

Using Boussinesq approximation with L as the length scale, L^2/κ as the time scale (κ is the thermal diffusivity), $T_h^* - T_0^*$ as the temperature scale, and $\kappa^2\rho_0/L^2$ as the pressure scale, the non-dimensional governing equations are

$$(\partial_t + \boldsymbol{u}\cdot\nabla)\boldsymbol{u} = -\nabla p + \sigma\nabla^2\boldsymbol{u} + N^2\,T\boldsymbol{e}_z, \tag{2}$$

$$(\partial_t + \boldsymbol{u}\cdot\nabla)T = \nabla^2 T, \qquad \nabla\cdot\boldsymbol{u} = 0, \tag{3}$$

where $\boldsymbol{u} = (u, v, w)$ is the velocity in cylindrical coordinates $(r, \theta, z) \in [0, A_r/A_z]\times[0, 2\pi]\times[0, 1] = \mathcal{D}$, the corresponding vorticity is $\boldsymbol{\omega} = \nabla\times\boldsymbol{u} = (\xi, \eta, \zeta)$, p is the dynamic pressure, $\boldsymbol{e}_z = (0, 0, 1)$ is the vertical unit vector in the z-direction and $T = (T^* - T_0^*)/(T_h^* - T_0^*)$ is the non-dimensional temperature, while T^* is the dimensional temperature. N^2 is the non-dimensional Brunt-Väisälä frequency $N^2 = N_{\rm BV}^2L^4/\kappa^2 = \sigma^2 A_T A_z^3 Gr$. The non-dimensional parameters are:

$$\begin{aligned}
&\text{Grashof number:} && Gr = \alpha g D^3(T_h^* - T_0^*)/\nu^2,\\
&\text{Prandtl number:} && \sigma = \nu/\kappa,\\
&\text{cylinder to hot spot radial ratio:} && A_r = R/D,\\
&\text{axial aspect ratio:} && A_z = L/D,\\
&\text{temperature ratio:} && A_T = (T_t^* - T_0^*)/(T_h^* - T_0^*),
\end{aligned} \tag{4}$$

where ν is the kinematic viscosity and g is the acceleration due to gravity.

The system has been solved using a second-order time-splitting method, with space discretized via a Galerkin-Fourier expansion in θ and Chebyshev collocation in r and z. For the solutions presented here, with $A_r = A_z = 2$ and $A_T = 1$, we have used up to $n_r = 256$ and $n_z = 128$ Chebyshev modes in the radial and axial directions and $n_\theta = 36$ azimuthal Fourier modes.

The governing equations and boundary conditions are invariant under arbitrary rotations around the cylinder axis and reflections about meridional planes. The action of the two symmetries in our problem is given by

$$SO(2): \quad \tau(R_\alpha)(u, v, w)(r, \theta, z, t) = (u, v, w)(r, \theta - \alpha, z, t), \tag{5a}$$

$$Z_2: \quad \tau(K_\beta)(u, v, w)(r, \theta, z, t) = (u, -v, w)(r, 2\beta - \theta, z, t), \tag{5b}$$

where α and β are arbitrary angles. Together they generate the group $O(2)$. In an isothermal ambient ($A_T = 0$), the symmetry breaking process preserves Z_2 parity and no spontaneous generation of swirl occurs (Lopez and Marques, 2013), whereas in a stratified ambient ($A_T > 0$), the symmetry-breaking process results in a rotating wave with the spontaneous generation of swirl (Marques and Lopez, 2014).

3 Results

3.1 Basic state: steady and axisymmetric

For Gr up to about 10^5, the flow is steady and axisymmetric. For the results presented here, we fix $A_r = 2$, $A_z = 2$, $A_T = 1$ and $\sigma = 7$; $A_T = 1$ means that the center of the hot

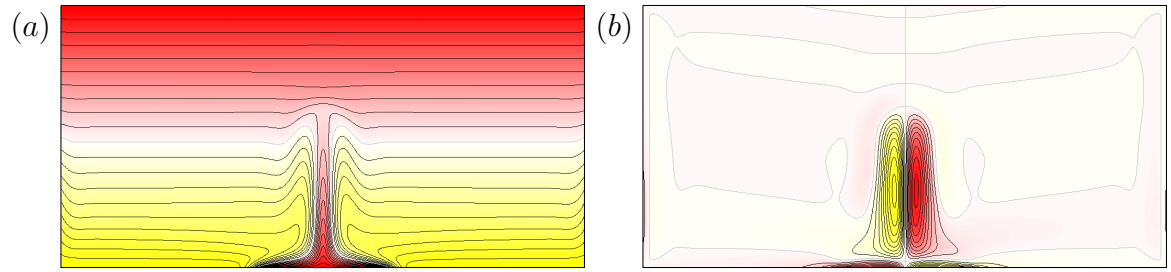

Figure 1: (a) Isotherms and (b) azimuthal vorticity contours of the steady axisymmetric basic state BS at $Gr = 10^5$.

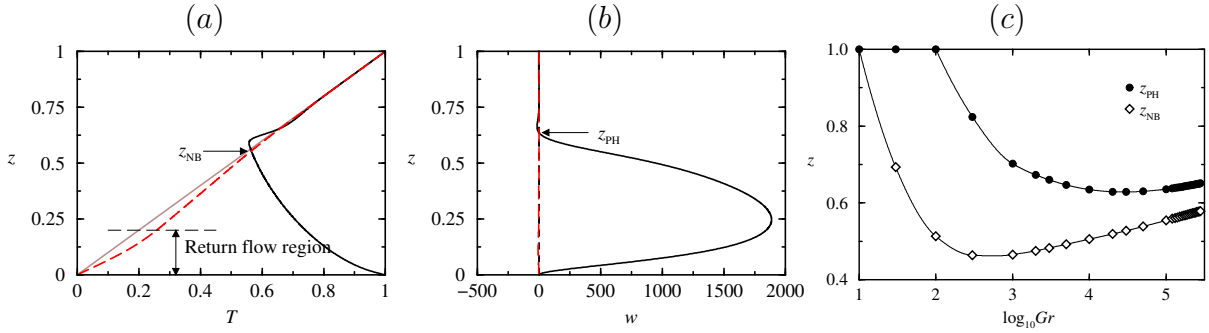

Figure 2: Profiles of (a) temperature $T(z)$ and (b) vertical velocity $w(z)$ of the steady axisymmetric basic state BS at $Gr = 10^5$, and (c) variation of the plume height, $z_{\rm PH}$, and neutral buoyancy level, $z_{\rm NB}$, with Gr.

spot on the bottom is at the same temperature as the top endwall, and so the neutral buoyancy level of a well-developed plume will be roughly half way between the top and bottom. The localized heating in the center of the bottom endwall means that there is a non-zero radial temperature gradient for any non-zero Gr. This radial temperature gradient locally produces azimuthal vorticity resulting in a meridional circulation drawing fluid radially inward above the heated portion of the bottom endwall and upward along the axis, eventually forming a thermal plume for larger Gr. The vertical extent of this axial plume is limited by the vertical stratification and the diffusion of both temperature and vorticity. Figure 1 illustrates this for $Gr = 10^5$.

Figure 2(a, b) shows vertical profiles at the axis of the temperature $T(r = 0, z)$ and the vertical velocity $w(r = 0, z)$. We have used such profiles for a quantitative measurement of the plume height, $z_{\rm PH}$, defined as the stagnation point of the plume where $w(r = 0, z_{\rm PH}) = 0$, and the neutral buoyancy level $z_{\rm NB}$, defined as the height at which the plume temperature (and density) equals the ambient temperature. The dashed line in figure 2(a) is the T-profile at mid-radius ($r = 0.5A_r$). Figure 2(c) shows the variations of $z_{\rm PH}$ and $z_{\rm NB}$ over a range of Gr for which the base state is stable. For small $Gr \lesssim 10^3$, the plume is not well-developed and so the plume height is ill-defined. The neutral buoyancy level is lower than the top endwall for $Gr > 10$ and decreases with increasing Gr for small Gr until the flow begins to undergo the transition from being conduction dominated to convection dominated and the plume begins to be well-established, at about $Gr = 300$. With further increases in Gr, the neutral buoyancy level grows monotonically with Gr. The plume height is always larger than the neutral buoyancy level, it decreases with increasing Gr

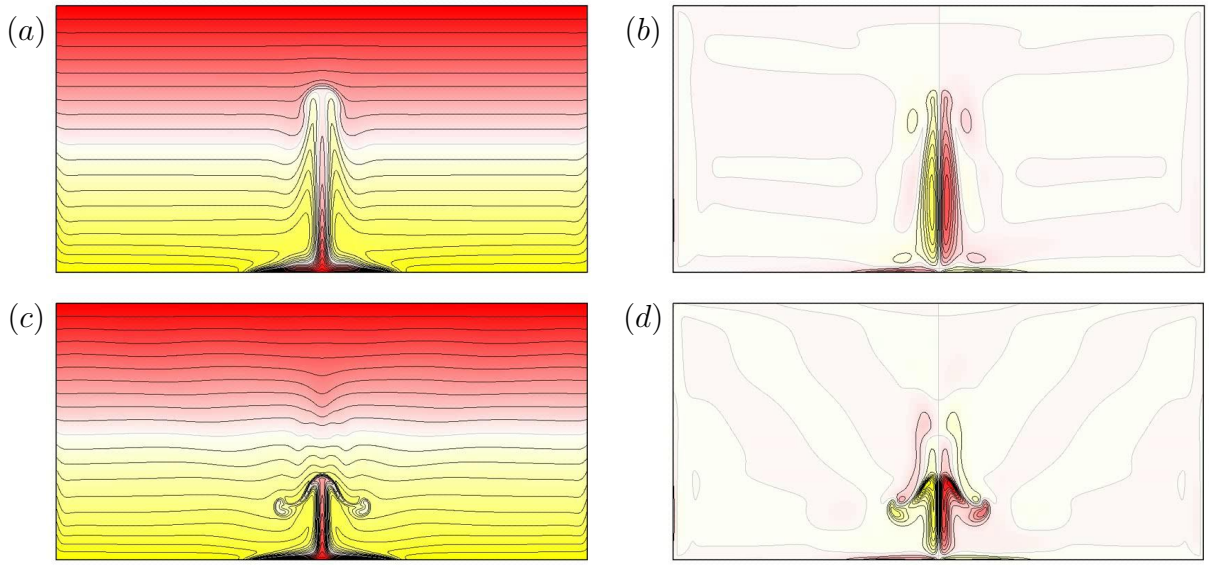

Figure 3: Isotherms (left) and azimuthal vorticity contours (right) of the axisymmetric periodic puffing plume state at (a, b) $Gr = 3.5 \times 10^5$ and (c, d) at $Gr = 10^6$.

until $Gr \approx 2 \times 10^4$, suggesting that the transition regime from conduction to convection dominated flow is broadly between $Gr = 300$ and $Gr = 2 \times 10^4$.

3.2 Axisymmetric puffing plume

With the simulations restricted to the axisymmetric subspace, the basic state loses stability via a supercritical Hopf bifurcation at $Gr \approx 2.84 \times 10^5$. The instability is due to the development of a buoyancy anomaly near the hot spot; this develops into a localized blob of fluid which rises faster than the fluid in the plume in the underlying unstable steady solution. This periodic flow is very much the same as in the non-stratified ambient localized heating problem (Lopez and Marques, 2013), the so-called puffing plume. Figure $3(a, b)$ shows a snap-shot at $Gr = 3.5 \times 10^5$; the movie in the presentation clearly shows the development of the puffs. For a range of Gr following the Hopf bifurcation, the puffing frequency, ω_0, grows monotonically with Gr, as does the buoyancy frequency N ($N \sim \sqrt{Gr}$). The puffing frequency is larger than N ($\omega_0 \sim 1.4N$), and so the puffing plume does not drive internal waves. At $Gr \approx 4.7 \times 10^5$, the puffing plume undergoes a period-doubling bifurcation: the blob in the plume develops into a vortex ring whose radius expands while the central plume column remains intact. At the next cycle the remains of the ring are still there, impeding the subsequent blob developing into a ring, and the blob instead travels up the central column which overshoots the neutral buoyancy level higher than in the previous cycle. The next cycle coincides with the previous one. Figure $3(c, d)$ shows a snap-shot of the period-doubled puffing plume at $Gr = 10^6$; the movie in the presentation clearly shows period-doubled dynamics. The period-doubling results in the frequency of the oscillation being smaller than N and internal waves are seen to emit from the head of the plume.

Figure 4 shows how the plume frequency varies with Gr, and compares it to N. For $Gr > 4.8 \times 10^5$, the flow is quite complicated temporally, becoming quasi-periodic and then synchronizing, then quasi-periodic again, with some very long period modulations

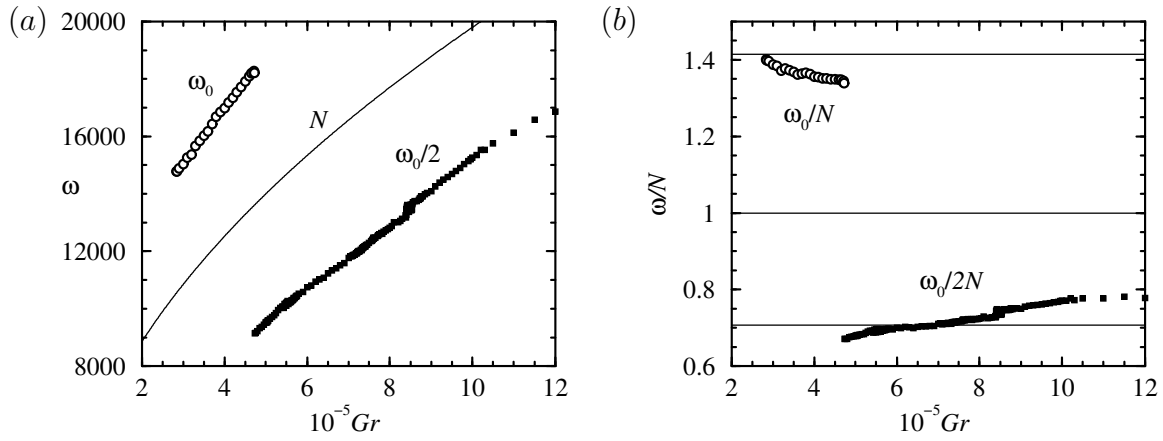

Figure 4: Variation of (a) the primary frequency of the axisymmetric puffing plumes ω versus Gr; the curve is the non-dimensional buoyancy frequency, N, the open symbols correspond to limit cycle puffing states and the filled symbols are various puffing states that are generally quasi-periodic, but some have frequency locked to being periodic. The puffing frequency is ω_0. Part (b) shows the same results scaled by N; the three horizontal lines are at $\omega_0/N = 2/\sqrt{2}$, 1, and $1/\sqrt{2}$.

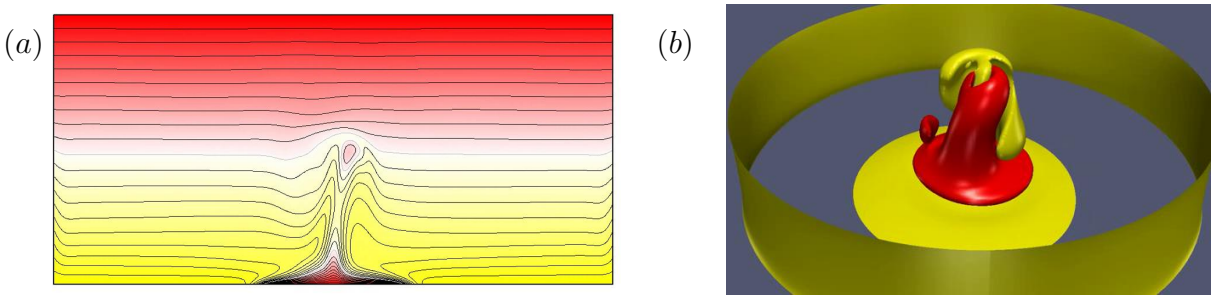

Figure 5: Snapshots of (a) isotherms and (b) azimuthal vorticity of the rotating wave state RW at $Gr = 2 \times 10^5$.

over short intervals in Gr, suggesting that there are resonant dynamics at play. Nevertheless, there is a strong temporal signal such that the associated frequency, $\omega_0/2$, results in internal waves at about 40° to the vertical. This angle comes from the dispersion relation for internal waves, and is given by $\arccos(\omega_0/2N)$, although in actuality it is the local buoyancy frequency rather than that corresponding to the imposed sidewall boundary temperature profile that is relevant. This is consistent with many experimental observations of internal waves emerging from regions with localized instabilities and turbulence into a stratified region having frequencies in a narrow band about the local buoyancy frequency divided by $\sqrt{2}$ (Munroe and Sutherland, 2014), and Sutherland and Linden (1998) have shown using a linear theory that internal waves within this band of frequencies are the most efficient in extracting energy from the turbulent region and transporting it through the stratified region. They also suggest that these waves feed back upon the turbulent region and modify its mean properties to the extent that waves in this preferred frequency band are further enhanced. Similar mechanisms seem to be in play in the puffing plume regime.

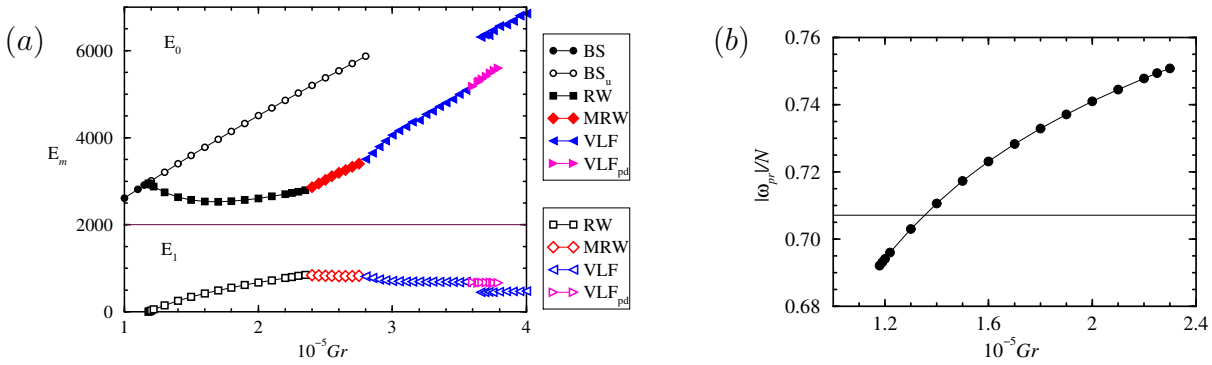

Figure 6: Variations with Gr of (a) the modal energies E_0 and E_1 (in azimuthal wavenumbers $m = 0$ and 1) of the various states as indicated, and (b) the precession frequency of RW scaled by N.

3.3 Spontaneous generation of swirl

When the simulations are not restricted and general three-dimensional perturbations are allowed, the base state BS loses stability at $Gr \approx 1.18 \times 10^5$, which is much lower than that for the onset of the axisymmetric puffing mode. The instability is via a supercritical Hopf bifurcation breaking the $SO(2)$ symmetry resulting in a pair of rotating waves (RW) with azimuthal wavenumber $m = 1$, one rotating in the positive, and the other in the negative azimuthal direction. Both are stable, and which is realized depends on initial conditons. The duality is due to the $O(2) = SO(2) \times Z_2$ symmetry of the system (Knobloch, 1996). An example of RW at $Gr = 2 \times 10^5$ is shown in figure 5. Figure 6(a) shows the modal energies E_0 and E_1 of the solutions obtained up to $Gr = 4 \times 10^5$. Figure 6(b) shows the variation of the absolute value of the precession frequency ω_{pr} with Gr, scaled by N. It shows that $|\omega_{pr}|/N \sim 1/\sqrt{2}$, and so internal waves are excited by the rotating wave state, RW, and are emitted at about 45°, much like the internal waves in the period-doubled axisymmetric puffing plume.

By further increasing the Grashof number, the rotating wave undergoes a sequence of bifurcations to more complicated time dependent states. The first bifurcation results in a quasiperiodic state, MRW. In the precessing frame, the plume is periodic, and the new periodicity corresponds to a puff of hot fluid propagating upwards along the tilted plume. The puffing frequency ω_{pu} is easily computed from the time series of the kinetic energy of MRW. Since the kinetic energy is a global measure, the precession frequency disappears from its time series and the energies are purely periodic. The result is $\omega_{pu} = 1.414 \times 10^4$, which is very close to, but not exactly equal to, twice the precession frequency ($2\omega_{pr} = 1.487 \times 10^4$). The puffing phenomena in MRW is closely related to the puffing we have observed when the computations are restricted to the axisymmetric subspace. This strongly suggests that the two puffing mechanisms, in the axisymmetric subspace and in the full 3D space, are the same. The axisymmetric puffing appears at $Gr \approx 2.84 \times 10^5$, while the puffing plume MRW appears at $Gr \approx 2.35 \times 10^5$. This fact, together with the proximity between ω_{pu} and $2\omega_{pr}$, suggests that the axisymmetric puffing mechanism is excited by the precessing plume before but close to it becoming unstable in the axisymmetric subspace, in an approximate 1:2 resonance between the puffing and the precessing frequencies.

By further increasing Gr, the quasiperiodic state MRW develops an additional very low

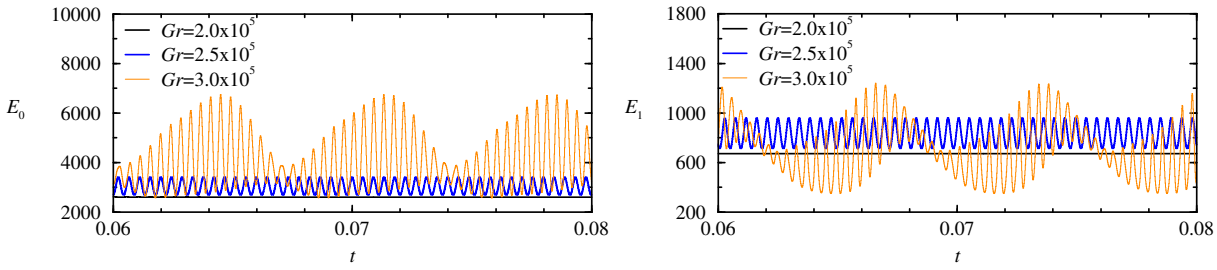

Figure 7: Time series of E_0 and E_1 for RW, MRW and VLF, at Gr as indicated.

frequency at about $Gr \approx 2.8 \times 10^5$. This new very low frequency state VLF is clearly apparent in figure 7, showing time series of E_0 and E_1 for the states RW and MRW that have already been described, and the new VLF state at $Gr = 3 \times 10^5$. At this particular Gr, the new frequency is about sixteen times smaller than the puffing frequency. Notice that the precession frequency does not appear in the energy time series because it is a global measure (integrating over the whole domain), and therefore the precession does not change the energy values. The VLF state, as is apparent from figure 7, alternates between a state very similar to the precessing puffing plume MRW (near the minima of E_0), and another state where the axisymmetric component measured by E_0 is substantially stronger, while the non-axisymmetric energy is smaller that that of MRW (near the maxima of E_0), i.e. they resemble axisymmetric puffing states. In fact, the axisymmetric puffing state emerges (in the axisymmetric subspace) at about the same value of Gr where the VLF state appears. This suggests that the VLF state is close to a heteroclinic cycle alternatively visiting the MRW solution (now unstable), and the axisymmetric puffing state (stable in the axisymmetric subspace, but unstable to 3D perturbations). The bifurcation giving rise to the VLF state would then be associated with the bifurcation producing the axisymmetric puffing state; it is a global bifurcation of heteroclinic type.

On further increasing Gr, the dynamics becomes more complicated; we have observed a period doubling of the VLF state and regions of coexistence of the VLF and MRW states, before the flow becomes temporally chaotic. These additional states have been included in figure 6 up to $Gr = 4 \times 10^5$, but we have not pursued further analysis of these complex states.

4 Conclusions

In order to investigate if the swirl arises due to extraneous effects (ambient rotation or ambient shear) or due to intrinsic effects, we have simulated the flow in a stationary fully enclosed cylinder driven by a localized hot spot at the bottom, in a stratified ambient that is maintained by a linearly decreasing fixed temperature up the sidewall. We fix the ratio of the temperature difference between the top and bottom of the sidewall to the temperature difference between the center of the hot spot and the bottom of the side to be $A_T = 1$ (resulting in the plume's neutral buoyancy level being at about the cylinder half-height), as well as fixing the geometry and fluid (water), and we explore the dynamics of the plume as the Grashof number Gr is increased. Increasing the Grashof number corresponds to increasing the temperature of the center of the hot spot relative to the temperature of the bottom of the sidewall, and since $A_T = 1$ this also means that the buoyancy frequency of the ambient stratification is increased proportionally with $\sqrt{Gr}$.

When the simulations are restricted to being axisymmetric, the steady plume flow loses stability to a puffing mode via a Hopf bifurcation at $Gr \approx 2.84 \times 10^5$. The steady axisymmetric plume state loses stability to three-dimensional disturbances at Gr significantly lower than the critical Gr for the axisymmetric puffing mode instability, at a parity-breaking Hopf bifurcation at $Gr \approx 1.18 \times 10^5$, resulting in the swirling plume. Near onset the swirling plume is a rotating wave and its precession frequency is about $1/\sqrt{2}$ times the buoyancy frequency, and so internal waves are emitted at about 45°. On further increasing $Gr > 2.4 \times 10^5$, the swirling plume is modulated. The modulation is due to a puff of hot fluid propagating upwards along the tilted swirling plume. We find that the precession frequency is exciting the puffing mode subharmonically at Gr values a little below where the puffing mode sets in in the absence of the swirl; the precession frequency is about half the puffing frequency. As Gr is increased beyond about 2.8×10^5, the plume is further modulated by a very low frequency. We show that this results from a global bifurcation and this very low frequency modulated plume is close to a heteroclinic cycle where the flow slowly drifts from a state resembling the axisymmetric puffing mode to a state resembling the rotating wave swirling plume. In summary, swirl results spontaneously from an intrinsic instability breaking parity symmetry. Subsequent instabilities lead to quite complicated spatio-temporal behavior. These results provides a new perspective with which to re-visit the question of how do naturally occurring plumes, such as dust devils, acquire their swirl.

Acknowledgements

This work was supported by the National Science Foundation grant CBET-1336410 and the Spanish Ministry of Education and Science grant FIS2013-40880.

References

Knobloch, E. (1996). Symmetry and instability in rotating hydrodynamic and magneto-hydrodynamic flows. *Phys. Fluids*, 8:1446–1454.

Lopez, J. M. and Marques, F. (2013). Instability of plumes driven by localized heating. *J. Fluid Mech.*, 736:616–640.

Marques, F. and Lopez, J. M. (2014). Spontaneous generation of a swirling plume in a stratified ambient. *J. Fluid Mech.*, 761:443–463.

Munroe, J. R. and Sutherland, B. R. (2014). Internal wave energy radiated from a turbulent mixed layer. *Phys. Fluids*, 26:096604.

Sutherland, B. R. and Linden, P. F. (1998). Internal wave excitation from stratified flow over a thin barrier. *J. Fluid Mech.*, 377:223–252.

Torrance, K. E. (1979). Natural convection in thermally stratified enclosures with localized heating from below. *J. Fluid Mech.*, 95:477–495.